UC Riverside
UC Riverside Previously Published Works

Title
Renormalization group approach to anisotropic superconductivity

Permalink
https://escholarship.org/uc/item/0207623b

Journal
Physical Review B - Condensed Matter and Materials Physics, 79(22)

ISSN
1098-0121

Authors
Roldán, R
Tsai, SW
López-Sancho, MP

Publication Date
2009-06-11

DOI
10.1103/PhysRevB.79.224514

Peer reviewed

Renormalization group approach to anisotropic superconductivity

R. Roldán,[1,2] Shan-Wen Tsai,[3] and M. P. López-Sancho[2]

[1]*Laboratoire de Physique des Solides, Université Paris-Sud, CNRS, UMR 8502, F-91405 Orsay Cedex, France*
[2]*Instituto de Ciencia de Materiales de Madrid, CSIC, Cantoblanco, E-28049 Madrid, Spain*
[3]*Department of Physics and Astronomy, University of California, Riverside, California 92521, USA*

The superconducting instability of the Fermi-liquid state is investigated by considering anisotropic electron-boson couplings. Both electron-electron interactions and anisotropic electron-boson couplings are treated with a renormalization group method that takes into account retardation effects. Considering a noninteracting circular Fermi surface, we find analytical solutions for the flow equations and derive a set of generalized Eliashberg equations. Electron-boson couplings with different momentum dependences are studied and we find superconducting instabilities of the metallic state with competition between order parameters of different symmetries. Numerical solutions for some couplings are given to illustrate the frequency dependence of the vertices at different coupling regimes.

PACS number(s): 74.20.Rp, 74.20.Fg, 74.25.Kc, 71.10.Hf

I. INTRODUCTION

Many-body interactions have important effects on the electronic properties of correlated materials and are subject of great attention. The main role played by the electron-phonon interaction in the conventional superconductivity (SC) has enhanced the interest in electron-boson coupling. In the formation of Cooper electron pairs in conventional superconductors the attractive pairing interaction is mediated by phonons as established by the Bardeen-Cooper-Schreiffer (BCS) theory of superconductivity. The Eliashberg theory[1,2] provides the appropriate equations to obtain the superconducting temperature at which pairing occurs, as well as the energy gap created in the electronic density of states (DOS). The Eliashberg equations describe an effective electron-electron interaction due to the exchange of any form of bosons. The Eliashberg function $\alpha^2 F(\omega)$, which gives the spectral electron-phonon density, and the Coulomb pseudo-potential μ^* (Anderson-Morel potential[3]), which characterize the pairing interaction, are input parameters of the Eliashberg equations.

Direct evidence that the bosons mediating the attractive interaction in conventional superconductors are phonons was provided by tunneling experiments.[4–6] Following the work of McMillan and Rowell,[5,7] by inversion of tunneling data, a unique value of $\alpha^2 F(\omega)$ as well of μ^* is provided by the structure in the electron-tunneling current measured as a function of the applied voltage, the dI/dV characteristic. For BCS superconductors the gap created in the DOS when pairing takes place is isotropic of s-wave symmetry. However, anisotropic electron-phonon coupling has been reported later on in some borocarbide material superconductors as YNi_2B_2C and $LuNi_2C$.[8,9] Furthermore the superconducting energy gap of MgB_2 was found to vary on the Fermi surface (FS) due to the momentum dependence of the electron-phonon interaction. The superconducting properties of this material, which present the highest superconducting transition temperature ($T_c = 39$ K) among the binary compounds,[10,11] are explained by the fully anisotropic Eliashberg theory[2,12] by including the momentum depen-

dence of the electron-phonon coupling combined with density-functional calculations.[13]

The anisotropic Eliashberg theory has also been applied to materials with other pairing symmetries[14,15] such as the copper oxides which present a $d_{x^2-y^2}$-wave order parameter. In this case, besides the phonons, other kinds of bosons have been considered, as for example, spin fluctuations.[16] In the copper oxides high-T_c superconductors there is currently not a consensus about the nature of the pairing interaction. The d-wave symmetry gap experimentally measured seems to favor a purely electronic pairing interaction. However a kink, i.e., a change in the slope in the quasiparticle energy dispersion has been reported by angle-resolved photoemission spectroscopy (ARPES) experiments[17] at an energy of about 50 meV. This kink could indicate a renormalization effect similar to that appearing in conventional superconductivity. In the cuprates, at this energy scale, there are multiple excitations such as phonons and spin fluctuations, which could be responsible for the renormalization. At a higher energy of 350 meV, other kinks have been reported related with bosonic excitations.[18] Both phonons[17] and spin fluctuations[19] have been proposed but the nature of the bosonic mode remains under debate. Therefore strong electron-electron correlations as well as strong electron-boson coupling have to be considered in order to analyze the experimental data.[20]

Experiments carried out by different techniques on hole-doped cuprates with oxygen isotope substitution (^{16}O-^{18}O) (Refs. 21–23) have claimed that phonons play an important role in cuprates. Recent data have provided evidence that the electron-phonon interactions are responsible for the origin of the nodal kink[24] confirming earlier ARPES results[25] which had indicated an anisotropic electron-phonon interaction in cuprates in both the normal and superconducting states. However, the mechanism of pairing in high-temperature superconductors is still under discussion.

We focus here on the study of the superconducting instability with pairing mediated by anisotropic electron-boson coupling. The most general case of anisotropic coupling of electrons to bosonic modes is considered with a combination of many symmetry channels. We follow the asymptotically

exact renormalization group (RG) approach developed in Ref. 26. This extension of the RG treats electron-electron and electron-phonon interaction on an equal footing. Analytical and numerical solutions of the flow equations for the BCS vertices are obtained. Generalized Eliashberg equations and the corresponding MacMillan-Rowell and Allen-Dynes expressions for T_c are derived from the RG flow equations. The Migdal theorem[27] assumed in the Eliashberg theory is understood in terms of a large-N expansion in the RG approach.[26] We include both retardation effects and the presence of multiple energy scales in the problem. Retardation effects in the one-dimensional (1D) Holstein-Hubbard model at half filling have been found to be important near the transition between spin-density wave (SDW) and charge-density wave (CDW) states.[28] The classical and quantum aspects of fermion-driven lattice instabilities have been analyzed using an extension of the RG method similar to the one followed in the present work.[29] The calculation of the gap and the structure of the phase diagram of 1D tight-binding models such as molecular crystal and Su-Schrieffer-Heeger models have been analyzed at the one-loop level.[29] Furthermore, RG methods have been recently used to study the Cooper instability in graphene.[30,31]

The paper is organized as follows. In Sec. II the RG analysis is developed. In Sec. III the generalized Eliashberg equations are discussed. Section IV addresses results obtained for electron-boson couplings with different angular dependences. Finally in Sec. V the work is summarized and some conclusions are given.

II. RENORMALIZATION GROUP ANALYSIS

The RG method for interacting electrons[32] is adopted here to analyze the instabilities of a two-dimensional (2D) Landau Fermi liquid (FL). We start from a given geometry of the Fermi surface of the noninteracting system and we treat the microscopic interactions within one-loop RG, which captures the essential physics of the problem. In this way assumption of a predetermined order parameter is not needed. Since we are interested in the superconducting instability, both electron-electron and electron-boson interactions have to be considered. Therefore we follow the asymptotically exact RG scheme extended to include interacting fermions coupled to bosonic modes.[26]

In the Wilson-type RG theory,[32] at a first step, the modes of the momentum space above a cutoff Λ are integrated out. The remaining phase space in a 2D system is a ring of radius k_F and width of 2Λ around the Fermi energy E_F. In the second step the equations are solved by a large-N method, with $N=E_F/\Lambda$, N being the number of patches at the Fermi surface. Here a 2D square lattice is considered at low fillings so that the FS has an almost circular shape. The interactions are parametrized by the on-site Coulomb repulsion u_0, the electron-boson coupling g, and the Einstein frequency ω_E of the bosons. In this case the electron-boson constant is $\lambda = 2N(0)g^2/\omega_E$, where $N(0)$ is the density of states at the Fermi level.

The RG equations are derived in the path-integral representation.[26] In order to obtain a combination of many

symmetry channels, the most general anisotropic electron-boson coupling $g(i,j)$ is considered. The electron-boson coupling can be integrated out exactly leading to an electron-electron effective problem with retarded interactions. The retarded electron-electron interaction has the form

$$\tilde{u}(4,3,2,1) = u(4,3,2,1) - 2g(1,3)g(2,4)D(1-3), \quad (1)$$

where the phonon propagator is

$$D(q) = \frac{\omega_{\mathbf{q}}}{\omega^2 + \omega_{\mathbf{q}}^2}. \quad (2)$$

We adopt the notation $q=(\omega,\mathbf{q})$, $1=(\omega_1,\mathbf{k}_1)$, and so forth. Spin indices are omitted in this notation. Particles 1 and 2 are incoming and scatter into 3 and 4, respectively. We will focus on processes involving particles with opposite spins. The processes involving particles with same spins can be obtained from these due to SU(2) symmetry.[33] For our almost circular FS the effective retarded electron-electron interaction $\tilde{u}$ gives two types of scatterings in the RG: the forward scattering, with $k_1=k_3$ and $k_2=k_4$, which, as in the case of pure electron-electron interaction, does not get renormalized but contributes to the electron self-energy, and the scattering in the Cooper channel. While the forward channel does not flow under the RG, the BCS vertex ($k_1=-k_2$, $k_3=-k_4$) flows at one loop in the RG equation

$$\frac{d}{d\ell}\tilde{u}(1,3,\ell) = -\int_{-\infty}^{\infty} \frac{d\omega}{\pi} \int_0^{2\pi} \frac{d\theta}{2\pi} \frac{\Lambda_\ell \tilde{u}(1,\omega,\theta,\ell)\tilde{u}(\omega,\theta,3,\ell)}{\Lambda_\ell^2 + Z_\ell^2(\omega,\theta)\omega^2},$$

$$(3)$$

where $1\equiv(\omega_1,\theta_1)$, $3\equiv(\omega_3,\theta_3)$, and ℓ represents the RG scale $\ell=\ln(\Lambda_0/\Lambda)$ with Λ_0 as the initial bandwidth. Equation (3) is obtained from the cutoff independent condition imposed to the interaction vertex

$$\frac{d}{d\ell}\tilde{u}(4,3,2,1) = 0. \quad (4)$$

The vertices are labeled according to the angle around the FS θ_i since the dependence on the radial part of the momentum is irrelevant here.[32] However, the dependence on the modulus $|\mathbf{q}|$ is important at larger fillings[34,35] where, in addition, electron-electron interactions may lead to renormalization of the FS shape.[36] In order to solve the differential Eq. (3) the pairing potential is decomposed in terms of the irreducible representation of the space group of the underlying lattice. For the case of a 2D square lattice the space group is D_4. The irreducible representations of the D_4 space group contain four one-dimensional (singlets): A_1 and A_2 for conventional and unconventional s-wave channels, B_1 for $d_{x^2-y^2}$ channel, and B_2 for d_{xy} channel and one two-dimensional (triplet): E corresponding to p-wave symmetry with degenerate eigenvalues for the two channels p_x and p_y. The corresponding basis functions are chosen to be

$$A_1 \quad \phi_n^1(\theta) = C_n \cos[4(n-1)\theta]$$

$$B_1 \quad \phi_n^2(\theta) = C_0 \cos[[4(n-1)+2]\theta]$$

$$B_2 \quad \phi_n^3(\theta) = C_0 \sin[[4(n-1)+2]\theta]$$

$$A_2 \quad \phi_n^4(\theta) = C_0 \sin[4n\theta]$$

$$E \quad \begin{cases} \phi_n^5(\theta) = C_0 \sin[(2n-1)\theta] \\ \phi_n^6(\theta) = C_0 \cos[(2n-1)\theta] \end{cases} \quad (5)$$

with n ranging from 1 to ∞, and the normalization factors $C_n = 1/\sqrt{\pi(1+\delta_{n1})}$. Therefore we can express the pairing potential in the more general form

$$\tilde{u}(i,j,\ell) = \sum_\gamma \sum_{m,n} u_{mn}^\gamma(\omega_i,\omega_j,l) f_{mn}^\gamma(\theta_i,\theta_j), \quad (6)$$

where γ labels the representation of the group and

$$f_{mn}^\gamma(\theta_i,\theta_j) = \phi_m^\gamma(\theta_i)\phi_n^\gamma(\theta_j), \quad (7)$$

where $\phi_m^\gamma(\theta)$ are the corresponding basis functions given in Eq. (5). The normalized basis functions $\phi_m^\gamma(\theta)$ are orthogonal

$$\int_0^{2\pi} \phi_m^\gamma(\theta)\phi_n^{\gamma'}(\theta)d\theta = \delta_{mn}\delta^{\gamma\gamma'} \quad (8)$$

and form a complete basis set. By discretizing the frequency integral into a sum, taking advantage of the orthogonality and completeness of the ϕ basis and restricting ourselves to frequencies below the cutoff, the two-dimensional matrix $\tilde{u}(i,j,\ell)$ expressed in Eq. (6) can be transformed into a four-dimensional tensor $[\hat{u}_{nm}^\gamma]_\beta^\alpha(\ell)$. Therefore we can rewrite the flow equation, Eq. (3), as a *tensor* equation

$$\frac{d}{d\ell}[\hat{u}_{nm}^\gamma]_\beta^\alpha(\ell) = -\sum_{\delta=-N}^{N}\sum_{i,j=0}^{M} [\hat{u}_{ni}^\gamma]_\delta^\alpha(\ell)[\hat{K}_{ij}^\gamma]_\delta^\delta(\ell)[\hat{u}_{jm}^\gamma]_\beta^\delta(\ell),$$

$$(9)$$

where we have imposed an upper limit to the harmonic index $n \leq M$, and to the frequency sum, $-N \leq \delta \leq N$. In Eq. (9) we have used

$$[\hat{u}_{nm}^\gamma]_\beta^\alpha(\ell) = \int d\theta_\alpha \int d\theta_\beta \tilde{u}(\alpha,\beta,\ell)\phi_n^\gamma(\theta_\alpha)\phi_m^\gamma(\theta_\beta),$$

$$[\hat{K}_{ij}^\gamma]_\beta^\alpha(\ell) = K_{ij}^\gamma(\omega_\alpha,\ell)\delta_\beta^\alpha, \quad (10)$$

with the kernel

$$K_{ij}^\gamma(\omega,\ell) = \int_0^{2\pi} d\theta \frac{\Lambda_\ell}{\Lambda_\ell^2 + Z_\ell^2(\omega,\theta)\omega^2}\phi_i^\gamma(\theta)\phi_j^\gamma(\theta). \quad (11)$$

Therefore Eq. (9) can be written in a compact form as a $(2N+1)M \times (2N+1)M$ matrix equation. The flow equation has the form

$$\frac{d\mathbf{U}^\gamma}{d\ell} = -\mathbf{U}^\gamma \cdot \mathbf{K}^\gamma \cdot \mathbf{U}^\gamma, \quad (12)$$

where the matrix indices j are related to the frequency α and harmonic n indices by $\alpha = \text{IP}[(j-1)/M]+1$ and $n = j-(\alpha-1)M$, respectively, where IP denotes the integer part. From Eq. (12) we obtain one vertex flow equation for each channel γ. Once we have the matrix form of the RG flow equations for the vertices it is possible to write the exact solution

$$\mathbf{U}^\gamma(\ell) = [\mathbf{1} + \mathbf{U}^\gamma(0)\cdot\mathbf{P}^\gamma(\ell)]^{-1}\cdot\mathbf{U}^\gamma(0), \quad (13)$$

where $\mathbf{P}^\gamma(\ell) \equiv \int_0^\ell d\ell' \mathbf{K}^\gamma(\ell')$. There is an instability of the Fermi-liquid state when $\mathbf{U}^\gamma(\ell_c) \to \infty$ for $\ell = \ell_c$. This condition is fulfilled when

$$\det[\mathbf{1} + \mathbf{U}^\gamma(0)\cdot\mathbf{P}^\gamma(l_c)] = 0, \quad (14)$$

which is equivalent to solving the eigenvalue equation

$$[\mathbf{1} + \mathbf{U}^\gamma(0)\cdot\mathbf{P}^\gamma(\ell_c)]\cdot\mathbf{v}^\gamma = 0. \quad (15)$$

The kernel $\mathbf{K}^\gamma(\ell)$ that appears in the vertex flow equations is given by Eq. (11) and contains self-energy corrections. The momentum-dependent imaginary part of the self-energy $\Sigma''(\omega,\mathbf{k})$, with contributions from all the components of the electron-boson coupling, is related to the quasiparticle weight by $\Sigma''(\omega,\theta) = [1-Z_\ell(\omega,\theta)]\omega$. The imaginary part of the self-energy is renormalized by the bare forward vertices and the flow equation for the quasiparticle weight $Z_\ell(\omega,\theta)$ can be integrated to give

$$Z_\ell(\omega_\alpha,\theta_\alpha) = 1 + \frac{2}{\pi\omega_\alpha}\int_{\Lambda_\ell}^{\Lambda_0} d\Lambda_{\ell'} \int d\theta_\beta d\omega_\beta$$

$$\times \frac{N(0)\tilde{u}_0(\alpha,\beta)Z_{\ell'}(\omega_\beta,\theta_\beta)\omega_\beta}{\Lambda_{\ell'}^2 + Z_{\ell'}^2(\omega_\beta,\theta_\beta)\omega_\beta^2}, \quad (16)$$

where $\tilde{u}_0(\alpha,\beta)$ is the retarded electron-electron interaction

$$\tilde{u}_0(\alpha,\beta) = u_0 - 2g^2(\theta_\alpha,\theta_\beta)D(\omega_\alpha - \omega_\beta). \quad (17)$$

The self-energy is angle dependent and it appears as a term in the denominator of $\mathbf{K}^\gamma(\ell)$. Therefore, whereas only the γ component $\mathbf{K}^\gamma(\ell)$ of the kernel contributes to a given channel γ, all γ components of the microscopic electron-boson coupling contribute to $\mathbf{K}^\gamma(\ell)$. The results of this section will be used in Sec. IV, where a numerical analysis of the RG flow equations as well as the $\lambda - W_c$ phase diagram are studied, W_c being the energy scale of the instability.

III. ELIASHBERG EQUATIONS

Eliashberg theory[1,2] of superconductivity was originally formulated to describe phonon-mediated s-wave superconductors. By including momentum dependence in the electron-boson interaction the anisotropic Eliashberg formalism is obtained. The Eliashberg function $\alpha^2F(\omega)$, which defines the electron-boson coupling $\lambda = 2\int_0^\infty \alpha^2F(\omega)d\omega/\omega$ carries, in the anisotropic formalism, momentum dependence. The fully anisotropic Eliashberg formalism has been successfully used to study the superconducting properties of MgB$_2$.

By solving numerically the anisotropic Eliashberg equations the superconducting transition temperature, the momentum-dependent superconducting energy gap, and the momentum-dependent specific heat have been obtained.[13,37] Generalization of the Eliashberg equations to d-wave superconductivity has as well been done[38] and has been used to investigate the physics of cuprates.[39] As it was shown in Ref. [26], the reduced Coulomb repulsion μ^* or Anderson-Morel potential emerges naturally from the RG equations as $\mu^* = u_0/(1 + \ell_E u_0)$, where $\ell_E = \ln(\Lambda_0/\omega_E)$. The value of T_c, and the analytical forms of the McMillan[7] and Allen-Dynes[40,41] expressions are obtained from the RG flow equations.

Here the instability conditions obtained in the Sec. II for the BCS vertex are mapped into the Eliashberg equations. The breakdown of the Fermi-liquid state by the SC instability due to the retarded electron-electron interactions occurs at a finite temperature which turns out to be the same critical temperature T_c obtained from the Eliashberg theory. To investigate this instability we solve the RG flow equations at finite temperature. Since the SC instability is approached by decreasing the temperature, in the equations such as (15), where integration over Λ is involved, this can be extended to zero. In this formalism, considering a finite value of the temperature T, the quasiparticle weight $Z_\ell(\omega, \theta)$ also presents a T dependence. Taken the appropriate integration limits in Eq. (16) we obtain a similar expression to Eq. (15), which gives the condition for the appearance of the instability and allows us to obtain the expression for T_c. The integrals over frequencies can be written as Matsubara sums $[\int d\omega_\beta/(2\pi) \rightarrow T_c \Sigma_\beta]$ in Eqs. (15) and (16) leading to

$$v^\gamma(\omega_n, \theta) = \pi T_c \sum_{\omega_m} \frac{1}{|\omega_m|} \int_{\theta'} \Gamma^\gamma_{\theta, \theta'}(\omega_n - \omega_m) \frac{v^\gamma(\omega_m, \theta')}{Z(\omega_m, \theta', T_c)},$$

$$Z(\omega_n, \theta, T_c) = 1 + \pi T_c \sum_{\omega_m} \bar{\Gamma}_\theta(\omega_n - \omega_m). \quad (18)$$

These two expressions are the set of generalized Eliashberg equations at T_c, where

$$\Gamma^\gamma_{\theta, \theta'}(\omega_\alpha - \omega_\beta) \equiv -\int_{\theta_\alpha, \theta_\beta} N(0)\tilde{u}_0(\alpha, \beta) \eta^\gamma(\theta_\alpha, \theta) \eta^\gamma(\theta_\beta, \theta')$$

$$\bar{\Gamma}_\theta(\omega_\alpha - \omega_\beta) \equiv -\int_{\theta_\beta} \frac{N(0)}{2\pi} \tilde{u}_0(\alpha, \beta) \quad (19)$$

with $\eta^\gamma(\theta_\beta, \theta) = \Sigma_{p=1}^\infty \phi_p^\gamma(\theta_\beta)\phi_p^\gamma(\theta)$. The u_0 term that appears in the definition of $\bar{\Gamma}_{\theta_\alpha}$ via $\tilde{u}_0$ does not contribute to Z because it does not have any dependence on frequency, and therefore the Matsubara sum in Eq. (18) vanishes for this term. The u_0 term in $\Gamma^\gamma_{\theta, \theta'}$ does however contribute to the Eq. (18) involving $v^\gamma(\omega_n, \theta)$. There is one such generalized Eliashberg equation for each channel γ, which depends on the γ component of the initial coupling through $\Gamma^\gamma_{\theta, \theta'}$ as defined in Eq. (19). However, each of these equations, corresponding to a particular channel γ, also depend on the quasiparticle weight Z which is renormalized by *all the*

components of the initial coupling through $\bar{\Gamma}_\theta$ as defined in Eq. (19).

From the generalized Eliashberg equations one can obtain the value of T_c in terms of the microscopic parameters. For the most general case, analytical expressions for T_c are quite involved. We consider first the special case in which $g(\theta_\alpha, \theta_\beta)$ is separable, so that it has the form $g(\theta_\alpha, \theta_\beta) = f(\theta_\alpha)f(\theta_\beta)$, and set $u_0 = 0$ for now. Then $\Gamma^\gamma_{\theta, \theta'}$ will also be separable

$$\Gamma^\gamma_{\theta, \theta'}(\omega_\alpha - \omega_\beta) = \Gamma^\gamma_\theta(\omega_\alpha - \omega_\beta)\Gamma^\gamma_{\theta'}(\omega_\alpha - \omega_\beta), \quad (20)$$

where

$$\Gamma^\gamma_\theta(\omega_\alpha - \omega_\beta) \equiv \int_{\theta_\alpha} f^2(\theta_\alpha)\sqrt{2N(0)D(\omega_\alpha - \omega_\beta)} \eta^\gamma(\theta_\alpha, \theta).$$

On the other hand, it is always possible to write

$$\bar{\Gamma}_\theta(\omega_\alpha - \omega_\beta) = \frac{1}{2\pi} \int_{\theta'} \bar{\Gamma}_\theta(\omega_\alpha - \omega_\beta)\bar{\Gamma}_{\theta'}(\omega_\alpha - \omega_\beta), \quad (21)$$

where $\bar{\Gamma}_\theta(\omega_\alpha - \omega_\beta) \equiv \Sigma_\gamma \Gamma^\gamma_\theta(\omega_\alpha - \omega_\beta)$. In the general case, since we know that $g(\theta_\alpha, \theta_\beta) = g(\theta_\beta, \theta_\alpha)$, we can use the decomposition $g(\theta_\alpha, \theta_\beta) = \Sigma_i f_i(\theta_\alpha)f_i(\theta_\beta)$, and therefore

$$\Gamma^\gamma_{\theta, \theta'}(\omega_\alpha - \omega_\beta) = \sum_i \Gamma^\gamma_{i\theta}(\omega_\alpha - \omega_\beta)\Gamma^\gamma_{i\theta'}(\omega_\alpha - \omega_\beta),$$

$$\bar{\Gamma}_\theta(\omega_\alpha - \omega_\beta) = \frac{1}{2\pi} \sum_i \int_{\theta'} \bar{\Gamma}_{i\theta}(\omega_\alpha - \omega_\beta)\bar{\Gamma}_{i\theta'}(\omega_\alpha - \omega_\beta). \quad (22)$$

The set of equations derived here reduce to those given by earlier treatment of Eliashberg theory for anisotropic electron-boson interaction by Daams and Carbotte,[42] if we consider a single separable channel $\gamma = 1$ and $n = 1$.

If for a given channel γ the gap is dominated by one component s such that the SC gap can be written as $\Delta_\gamma(\theta) = \Delta_0 \phi_s^\gamma(\theta)$ then the corresponding McMillan expression[7] for T_c becomes

$$T_c^\gamma \approx \omega_E \exp\left\{ \frac{Z_\gamma}{\mu^* \delta_{\gamma 1} - \lambda_\gamma} \right\} \quad (23)$$

where $\delta_{\gamma 1}$ restricts the contribution of μ^* to the channel $\gamma = 1$ (u_0 only has first harmonic of s-wave component), $Z_\gamma^{-1} = \int_\theta \phi_q^\gamma(\theta)/[1 + \bar{\lambda}(\theta)]$ and

$$\lambda_\gamma = Z_\gamma \sum_p \int_{\theta_\alpha, \theta_\beta, \theta} \frac{\lambda(\theta_\alpha, \theta_\beta)\phi_p^\gamma(\theta_\alpha)\eta^\gamma(\theta_\beta, \theta)\phi_q^\gamma(\theta)}{1 + \bar{\lambda}(\theta)} \quad (24)$$

with $\lambda(\theta_\alpha, \theta_\beta) \equiv 2N(0)g^2(\theta_\alpha, \theta_\beta)/\omega_E$ and $\bar{\lambda}(\theta) \equiv (2\pi)^{-1}\int_{\theta'}\lambda(\theta, \theta')$. The corresponding Allen-Dynes expression is

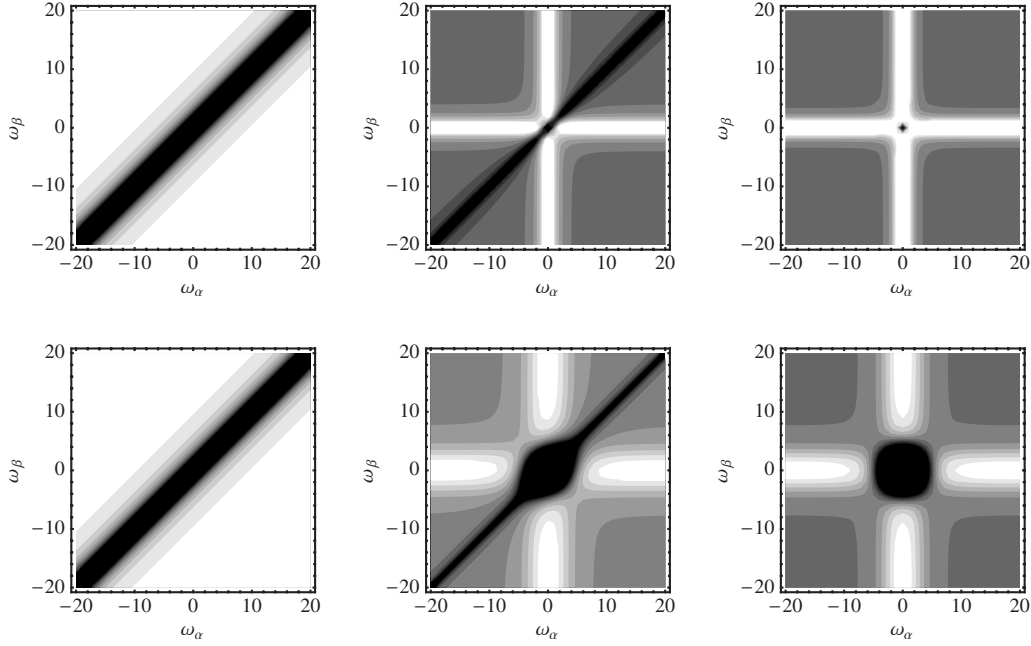$$T_c \approx \sqrt{\bar{\lambda}_\gamma}\omega_E, \quad (25)$$

where

FIG. 1. Plots of the $(2N+1)M \times (2N+1)M$ matrix $\mathbf{U}^\gamma(\ell)$ at different RG scales ℓ for the s channel ($\gamma=1$) and for the electron-boson coupling $g(\theta,\theta')=g_0 \cos(\theta-\theta')$. Here, for the first harmonic in the expansion ($M=1$), the number of frequency divisions is 41 ($N=20$) and $\Lambda_0=100$, $\omega_E=10$, and $u_0=0.1$. The three panels on the top correspond to $\lambda=0.4$ (weak coupling) and the three on the bottom correspond to $\lambda=4$ (strong coupling).

$$\bar{\lambda}_\gamma \equiv \sum_p \int_{\theta_\alpha,\theta_\beta,\theta} \lambda(\theta_\alpha,\theta_\beta) \phi_p^\gamma(\theta_\alpha) \eta^\gamma(\theta_\beta,\theta) \phi_q^\gamma(\theta). \quad (26)$$

The effective electron-phonon parameter λ_γ [Eq. (24)] that appears in the McMillan and Allen-Dynes equations for a particular channel γ does include contributions from *all components* of the bare coupling $\lambda(\theta_\alpha,\theta_\beta)$ through Z_γ and $\bar{\lambda}(\theta)$.

IV. NUMERICAL RESULTS

The method used allows for an easy numerical calculation of the critical temperature T_c (as well as the zero-temperature gap Δ_0) from the microscopic parameters u_0, $\lambda(\theta_\alpha,\theta_\beta)$, and ω_E. Equation (13) gives the RG evolution of all the vertices and can be evaluated at different RG steps ℓ. To find the instability one can simply calculate the quantity $\det[1+\mathbf{U}^\gamma(0)\cdot\mathbf{P}^\gamma(\ell)]$ and see when it approaches zero. Here we study electron-boson couplings with different angular dependences and strengths, going from the weak to the strong-coupling regimes. We label θ as the angle associated to $\mathbf{k} \equiv \mathbf{k}_1=-\mathbf{k}_2$ in polar coordinates, and θ' as the angle of $\mathbf{k}' \equiv \mathbf{k}_3=-\mathbf{k}_4$. In general we define $g(\theta,\theta')=g_0 f(\theta,\theta')$, where g_0 is a position-independent constant and the function $f(\theta,\theta')$ contains the full angular dependence of the electron-boson matrix elements. We consider two different cases: (a) the electron-boson coupling only depends on the difference between the angles of the electrons, (b) the coupling depends on the exact position of each of the electrons on the Fermi surface.

A. Solution of the RG flow equations for $g(\theta,\theta')=g_0 \cos(\theta-\theta')$

For this kind of angular dependence, the strength of the electron-boson coupling does not depend on the specific po-

sition of the particles on the FS but only depends on their relative orientation. By solving Eq. (14) we obtain the evolution of $\mathbf{U}^\gamma(\ell)$ with ℓ. For the coupling $g(\theta,\theta')=g_0 \cos(\theta -\theta')$, only three channels contribute, corresponding to s, $d_{x^2-y^2}$, and d_{xy} symmetries, respectively. Furthermore, the contributions of the two channels with d symmetry have the same magnitudes, the channels are degenerate, and we will generically refer to them as d-wave channel. In Fig. 1 the evolution of $\mathbf{U}^\gamma(\ell)$ with ℓ for the s channel is depicted. Each panel represents the $(2N+1)M \times (2N+1)M$ metric $\mathbf{U}^s(\ell)$ at a given RG step ℓ. The matrix elements corresponding to small frequencies around $\omega=0$ are at the center of the panels. The three top panels of Fig. 1 show the RG flow evolution for a case in the weak-coupling regime ($\lambda=0.4$). The first panel on the left shows the initial condition for which $\ell=0$. The third one, on the right-hand side, shows the vertices at $\ell=\ell_c$ right before the instability. We see that the most divergent couplings are those with frequencies below the Einstein frequency $|\omega_\alpha|,|\omega_\beta| < \omega_E$. In this case, simple two-step RG can be applied. The three panels on the bottom of Fig. 1 represent the evolution of the couplings for the strong electron-boson interaction regime ($\lambda=4$). In this case, the most divergent couplings (at $\ell=\ell_c$) are those with frequencies below a given energy scale $W_c > \omega_E$. As expected, these results are similar to that obtained in Ref. 43 where an isotropic electron-boson coupling was considered. Furthermore, this can be seen as a proof of the validity of our method, which matches the results of the isotropic limit when only the s channel is considered.

The situation is quite different for the d channel as it can be seen in Fig. 2. Again, the panels on the top correspond to the weak-coupling regime. The initial condition is the same as for the s channel, with the $u^d(\omega,-\omega,\ell=0)$ being the larg-
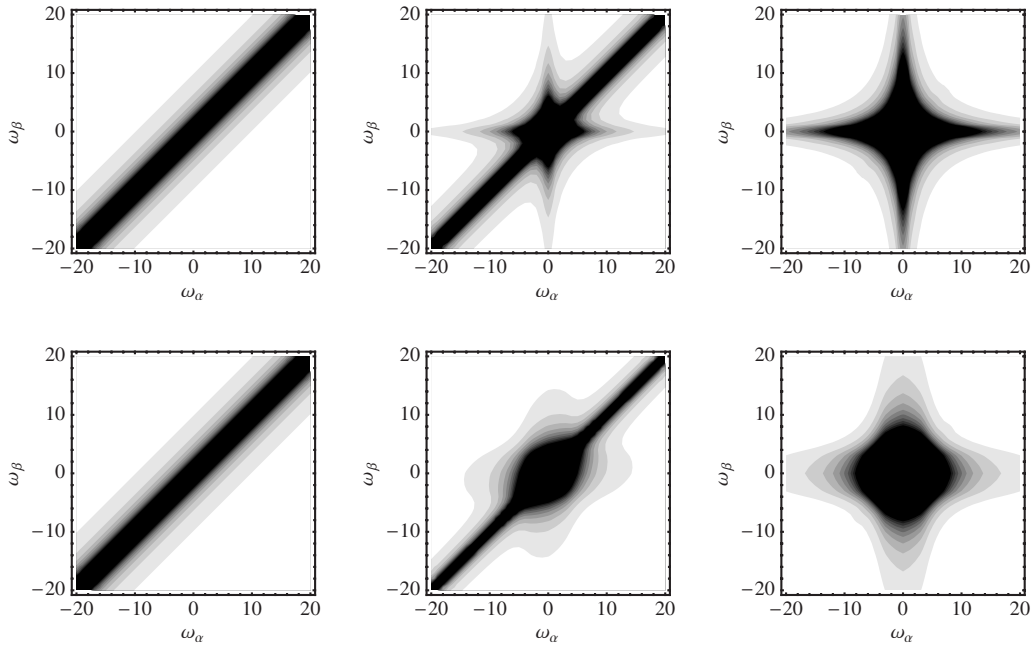
FIG. 2. Same as Fig. 1 but for the d channel ($\gamma = 2, 3$). The three panels on the top are for weak coupling ($\lambda = 0.4$) and the ones on the bottom are for the strong-coupling regime ($\lambda = 4$).

est couplings. However, close to the instability, the couplings $u^d(\omega_\alpha, \omega_\beta, \ell_c)$ that first diverge correspond to a region of frequencies centered around $\omega = 0$ and with a starlike shape. This frequency dependence of u^d at the instability point illustrates the importance of retardation effects in the RG flow. To have a physical understanding of this specific structure is, however, not trivial and we do not speculate here about the possible physical consequences of such dependence. On the other hand, the bottom panels of Fig. 2 represent the flow in the strong-coupling regime from the initial condition $\ell = 0$ to the critical RG step ℓ_c. In this case, the most divergent couplings at the instability point are, as in the s-wave case, those with frequencies below W_c.

In Fig. 3 we show the density plots of the matrix $\mathbf{U}^s(\ell_c)$ at the RG scale ℓ_c, where the instability appears for different values of the electron-boson coupling strength. At this point we can see more clearly how the energy scale separating high and low-energy physics moves from the Einstein frequency ω_E, in the weak-coupling regime to the critical cutoff W_c in the strong-coupling regime. The scale W_c can be associated with the $T = 0$ superconducting gap Δ_0, or with the

critical temperature T_c of the SC phase in the finite-temperature formalism.[26,43] Figure 3 also illustrates the breakdown of the two-step RG. In this approximation the vertex is chosen to be just the electron-electron part for frequencies above the Einstein frequency and to have some constant contributions from the boson modes for frequencies below ω_E.[44] This approximation works well in the weak-coupling limit, where the most divergent couplings are those with frequencies below ω_E. But for large $\lambda (\lambda \gg 1)$ this behavior breaks down and the scale for the divergent central region is on the order of $W_c > \omega_E$.

Similarly, the couplings $\mathbf{U}^d(\ell_c)$ in the d channel are shown in Fig. 4, from the weak to the strong electron-boson coupling regimes. We obtain the starlike structure at weak-coupling ($\lambda = 1$) evolving toward a more circular form in the strong coupling ($\lambda = 6$). More analytical studies are required for a full understanding of these patterns.

Figure 5 shows the energy scale W_c, where the SC instability occurs, as a function of the strength of electron-boson coupling λ at fixed ω_E. The two channels (s and d) that contribute to the electron-boson coupling $g(\theta, \theta')$
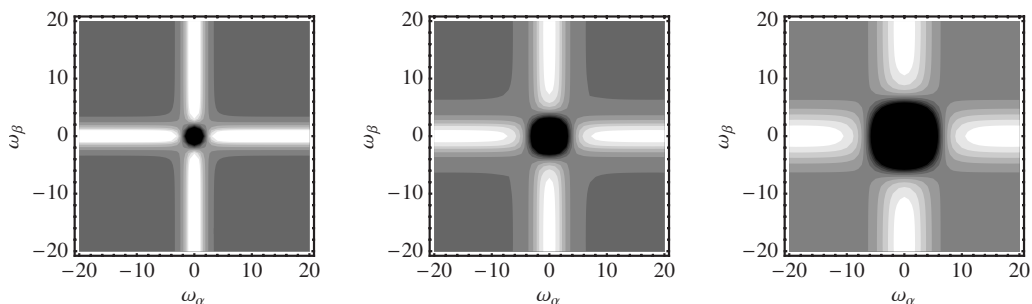

FIG. 3. Coupling matrix $\mathbf{U}^s(\ell_c)$ at the instability point for the s channel, from weak to strong coupling, for $u_0 = 0.1$. The corresponding electron-boson coupling is $g(\theta, \theta') = g_0 \cos(\theta - \theta')$. Panels correspond, from left to right, to $\lambda = 1, 2.5, 6$.
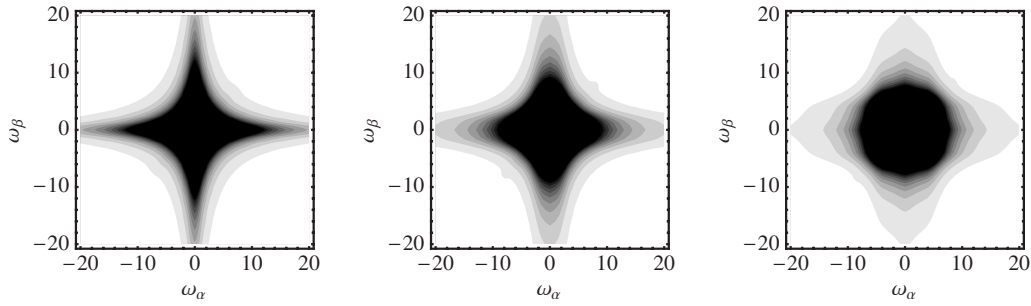
FIG. 4. Same as Fig. 3 and for the same parameter values, but for the d channel, $\mathbf{U}^d(\ell_c)$.

$=g_0 \cos(\theta - \theta')$, are represented. The behavior of W_c in the weak-coupling limit follows the McMillan exponential behavior of Eq. (23). For large λ strong-coupling regime, the W_c follows the Allen-Dynes law, Eq. (25). In the inset of Fig. 5 we show the phase diagram of the system. At finite temperature, the Fermi-liquid phase breaks down toward d-wave SC in the weak to intermediate coupling range and toward s-wave SC in the intermediate to strong-coupling regime. The larger the on-site electronic repulsion u_0, the larger the electron-boson coupling crossover between s-wave and d-wave superconductivity. This is expected since an isotropic u_0 only suppresses the contribution to the s-wave channel without affecting the other channels. Therefore for $u_0 = 0$, superconductivity only occurs in the s channel. Notice that, because the Kohn-Luttinger effect is not included in this one-loop RG calculation, there is no superconducting instability when only electron-electron repulsion is considered. In addition, this effect should shift the transition between d-wave and s-wave superconductivity toward some different value of the electron-boson coupling λ. The qualitative behavior is, however, well captured by our approximation, as shown in the phase diagram of Fig. 5.

B. Solution of the RG flow equations for $g(\theta, \theta') = g_0 \cos(\theta/2)\cos(\theta'/2)$

In the following we consider an electron-boson coupling with the angular dependence $g(\theta, \theta') = g_0 \cos(\theta/2)\cos(\theta'/2)$.
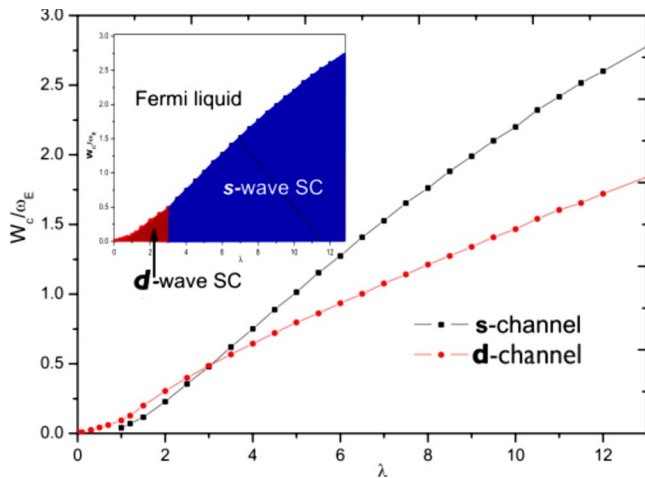

FIG. 5. (Color online) Critical cutoff W_c versus λ for the s channel (black squares) and the d channel (red circles). The values of the parameters used are $\Lambda_0 = 100$, $\omega_E = 10$, and $u_0 = 2.0$. The inset represents the phase diagram.

Unlike the previous case, this is a simple example for which the boson mode couples differently to electrons in different parts of the Fermi surface. That is, the coupling depends on the specific position of each of the electrons in the Fermi surface. As before, we obtain the ℓ evolution of $\mathbf{U}^\gamma(\ell)$ by solving Eq. (14) for this coupling. The two contributing channels in this case are of s and p symmetry. The evolution of $\mathbf{U}^p(\ell)$ for the p channel at weak electron-boson coupling shows a star-shaped structure, as it was found in Sec. IV A for the d channel. The frequency dependence of the coupling matrix close to the instability is very similar to that represented in the top right panel of Fig. 2.

In Fig. 6, the density plots of $\mathbf{U}^s(\ell_c)$ are shown for $u_0 = 0.1$ and different values of λ at the critical RG step ℓ_c. They present the same qualitative behavior as the corresponding s-channel results of the previous subsection (see Fig. 4). For the p channel, the density plots of the coupling matrix $\mathbf{U}^p(\ell_c)$ at the instability point ℓ_c are depicted in Fig. 7. The plot for $\lambda = 1.0$ is very similar to that obtained for the d channel in the case of a coupling of the form $g \propto \cos(\theta - \theta')$. This can be observed by comparing the left-hand side graphs of Figs. 4 and 7. However, the situation is different in the strong-coupling limit. The corresponding plot for the d channel shows that the most diverging matrix elements lie in a circular shaped region around $\omega = 0$ (see the right panel of Fig. 4). However in the present case, where $g \propto \cos(\theta/2)\cos(\theta'/2)$, the diverging matrix elements for the p channel are confined in a square region around $\omega = 0$, as shown in Fig. 7. This different behavior in the strong-coupling region needs a better understanding.

Finally we mention that it is possible to build a phase diagram similar to that of Fig. 5, but for a coupling of the form $g \propto \cos(\theta/2)\cos(\theta'/2)$. In this case, instead of having a low-coupling d-wave SC region in the phase diagram, we obtain a zone with p-wave pairing SC. For a value of $u_0 = 0.5$, the crossover between p and s wave superconductivity occurs at $\lambda \sim 2.5$. For a small value of the on-site Coulomb interaction $u_0 = 0.1$ it is found that the Fermi-liquid state is unstable toward p-wave SC in the range $0 < \lambda \lesssim 0.7$, and toward s-wave SC for larger values of the coupling, $\lambda \gtrsim 0.7$.

V. CONCLUSIONS

In this work we have investigated the pairing instabilities of the FL state which appear when the electron-boson coupling overcomes the effective repulsive electron-electron interaction. The most general case of anisotropic coupling of
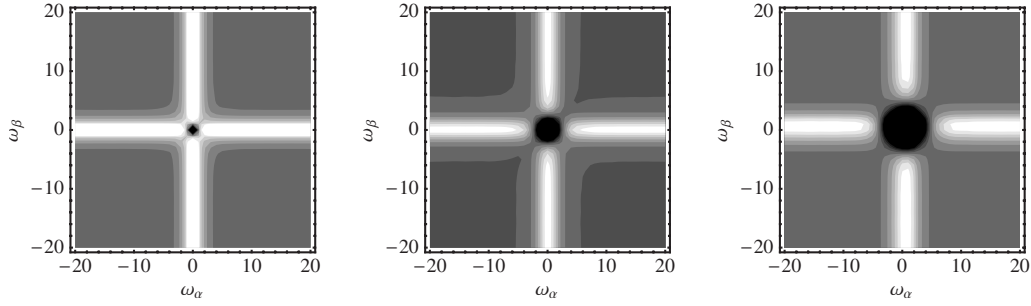
FIG. 6. Coupling matrix $\mathbf{U}^s(\ell_c)$ at the instability point for the s channel, from weak to strong coupling, for $u_0=0.1$. The corresponding electron-boson coupling is $g(\theta,\theta')=g_0\cos(\theta/2)\cos(\theta'/2)$. Panels correspond, from left to right, to $\lambda=1,2.5,6$.

electrons to bosons has been considered. The anisotropic boson exchange couplings are treated by an RG approach. Calculations are made for a 2D square lattice at low fillings. Under this assumption the system presents an almost circular FS, which allows for an analytical solution of the RG flow equations. Furthermore, the numerical evaluation of the flows provides information of the change in the frequency dependence of the vertices. The flow equations for the BCS vertex are decomposed into contributions coming from different symmetry channels with different angular momentum dependences. By varying the strength of the interaction from the weak to the strong-coupling regime the evolution of the couplings for the different symmetry channels is obtained. Channels of s, p, and d symmetries have been investigated.

We have considered here simple functional forms of the electron-boson couplings, such as $g(\theta,\theta')=g_0\cos(\theta-\theta')$, where the momentum of the exchanged boson only depends on the angle difference between the two electrons involved, and $g(\theta,\theta')=g_0\cos(\theta/2)\cos(\theta'/2)$, where the coupling depends explicitly on the position of each of the electrons on the Fermi surface. It is found that, even with these simple angular dependences, the anisotropic electron-boson couplings induce new nontrivial physics. . Although academic at first view, this problem makes contact with the physics which appears in some new anisotropic materials as those described in the introduction. In these materials such as metal-transition borocarbides, boronitrides, magnesium diboride, or cuprates, standard BCS theory cannot explain many of their properties. A consistent description of some physical behaviors is however achieved if anisotropy of the electron-boson coupling is included in the Eliashberg theory.[8,2,25] In

high-temperature superconductors there is a considerable amount of data that point to the interplay between electronic and atomic degrees of freedom.[45] The different behaviors shown by the quasiparticles in both nodal and antinodal regions of the Brillouin zone has suggested among other explanations, an anisotropic electron-phonon coupling alongside other many-body effects in order to understand the pairing mechanism.[46] Coupling to the half-breathing mode in the nodal region and to the buckling mode in the antinodal direction have been proposed as an interpretation to the renormalization effects seen in ARPES results in both the normal and superconducting phases.[25] However, more works are needed to get insight in the complex interplay between electron-boson interactions and electronic correlation in unconventional superconductivity.

In summary, we have studied the superconducting instability of the Fermi-liquid phase, considering electron-boson couplings with different angular dependences and strengths. SC order parameters of s, p, and d symmetries have been obtained depending on the anisotropy of the coupling and the strength of the interaction. The investigation of the frequency dependence of the couplings of different symmetries could be interesting in order to analyze and understand the complex behavior revealed by the experiments. Therefore, numerical evaluation of the RG flow equations is instructive in determining the range of important frequencies in different regimes and for different symmetry channels. Furthermore, at the instability point and for finite temperatures, the RG equations give the solution of the generalized Eliashberg equations at T_c and consequently McMillan and Allen-Dynes expressions have been obtained.
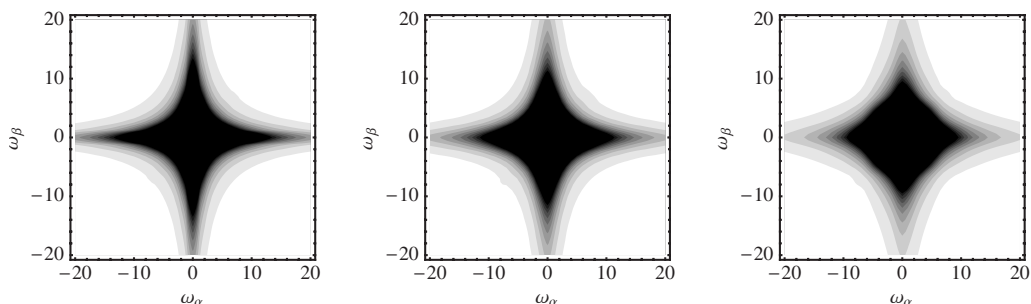

FIG. 7. Same as Fig. 6 and for the same parameter values, but for the p channel, $\mathbf{U}^p(\ell_c)$.

[1] G. M. Eliashberg, Zh. Eksp. Teor. Fiz. **38**, 966 (1960).

[2] J. P. Carbotte, Rev. Mod. Phys. **62**, 1027 (1990).

[3] P. Morel and P. W. Anderson, Phys. Rev. **125**, 1263 (1962).

[4] W. L. McMillan and J. M. Rowell, Phys. Rev. Lett. **14**, 108 (1965).

[5] W. L. McMillan and J. M. Rowell, in *Superconductivity*, edited by R. D. Parks (Dekker, New York, 1969), Vol. 1.

[6] D. J. Scalapino, in *Superconductivity*, edited by R. D. Parks (Dekker, New York, 1969), Vol. 1.

[7] W. L. McMillan, Phys. Rev. **167**, 331 (1968).

[8] S. Manalo, H. Michor, M. El-Hagary, G. Hilscher, and E. Schachinger, Phys. Rev. B **63**, 104508 (2001).

[9] S. Manalo and E. Schachinger, J. Low Temp. Phys. **123**, 149 (2001).

[10] C. Buzea and T. Yamashita, Supercond. Sci. Technol. **14**, R115 (2001).

[11] J. Nagamatsu, N. Nakagawa, T. Muranaka, Y. Zenitani, and J. Akimitsu, Nature (London) **410**, 63 (2001).

[12] P. B. Allen and B. Mitrovic, in *Solid State Physics*, edited by H. Ehrenreich, F. Seit, and D. Turnbull (Academic, New York, 1982), Vol. 37.

[13] H. J. Choi, D. Roundy, H. Sun, M. Cohen, and S. Louie, Nature (London) **418**, 758 (2002).

[14] A. J. Millis, S. Sachdev, and C. M. Varma, Phys. Rev. B **37**, 4975 (1988).

[15] A. V. Balatsky and J.-X. Zhu, Phys. Rev. B **74**, 094517 (2006).

[16] A. J. Millis, Phys. Rev. B **45**, 13047 (1992).

[17] A. Lanzara *et al.*, Nature (London) **412**, 510 (2001).

[18] T. Valla, T. E. Kidd, W. G. Yin, G. D. Gu, P. D. Johnson, Z. H. Pan, and A. V. Fedorov, Phys. Rev. Lett. **98**, 167003 (2007).

[19] S. V. Borisenko, A. A. Kordyuk, T. K. Kim, A. Koitzsch, M. Knupfer, M. S. Golden, J. Fink, M. Eschrig, H. Berger, and R. Follath, Phys. Rev. Lett. **90**, 207001 (2003).

[20] C. Honerkamp, H. C. Fu, and D. H. Lee, Phys. Rev. B **75**, 014503 (2007).

[21] G.-H. Gweon, T. Sasagawa, S. Zhou, and J. Graf, H. takagi, D.-H. Lee, and A. Lanzara, Nature (London) **430**, 187 (2004).

[22] J. Lee *et al.*, Nature (London) **442**, 546 (2006).

[23] R. Khasanov, S. Strassle, K. Conder, E. Pomjakushina, A. Bussmann-Holder, and H. Keller, Phys. Rev. B **77**, 104530 (2008).

[24] H. Iwasawa *et al.*, Phys. Rev. Lett. **101**, 157005 (2008).

[25] T. P. Devereaux, T. Cuk, Z.-X. Shen, and N. Nagaosa, Phys. Rev. Lett. **93**, 117004 (2004).

[26] S.-W. Tsai, A. H. Castro Neto, R. Shankar, and D. K. Campbell, Phys. Rev. B **72**, 054531 (2005).

[27] A. B. Migdal, Zh. Eksp. Teor. Fiz. **34**, 1438 (1958).

[28] K.-M. Tam, S.-W. Tsai, D. K. Campbell, and A. H. Castro Neto, Phys. Rev. B **75**, 161103(R) (2007).

[29] H. Bakrim and C. Bourbonnais, Phys. Rev. B **76**, 195115 (2007).

[30] C. Honerkamp, Phys. Rev. Lett. **100**, 146404 (2008).

[31] J. Gonzalez, Phys. Rev. B **78**, 205431 (2008).

[32] R. Shankar, Rev. Mod. Phys. **66**, 129 (1994).

[33] D. Zanchi and H. J. Schulz, Phys. Rev. B **61**, 13609 (2000).

[34] F. Guinea, R. S. Markiewicz, and M. A. H. Vozmediano, Phys. Rev. B **69**, 054509 (2004).

[35] T. Nishine, M. Tsuchiizu, and Y. Suzumura, J. Phys.: Conf. Ser. **132**, 012020 (2008).

[36] R. Roldán, M. P. López-Sancho, F. Guinea, and S.-W. Tsai, Phys. Rev. B **74**, 235109 (2006).

[37] H. J. Choi, M. L. Cohen, and S. G. Louie, Phys. Rev. B **73**, 104520 (2006).

[38] C. Jiang, E. Schachinger, J. P. Carbotte, D. Basov, and T. Timusk, Phys. Rev. B **54**, 1264 (1996).

[39] E. Schachinger and J. P. Carbotte, Phys. Rev. B **77**, 094524 (2008).

[40] C. R. Leavens and J. P. Carbotte, Can. J. Phys. **49**, 724 (1971).

[41] P. B. Allen and R. C. Dynes, Phys. Rev. B **12**, 905 (1975).

[42] J. M. Daams and J. P. Carbotte, J. Low Temp. Phys. **43**, 263 (1981).

[43] S.-W. Tsai, A. H. Castro Neto, R. Shankar, and D. K. Campbell, Philos. Mag. **86**, 2631 (2006).

[44] J. Polchinski, Nucl. Phys. B **422**, 617 (1994).

[45] F. Carbone, D. S. Yang, and A. H. Zwail, Proc. Natl. Acad. Sci. U.S.A. **105**, 20161 (2008).

[46] E. G. Maksimov, M. L. Kulc, and O. V. Dolgov, arXiv:0810.3789 (unpublished).